Appl. Math. Mech. -Engl. Ed., **44**(7), 1101–1110 (2023)

APPLIED MATHEMATICS AND MECHANICS (ENGLISH EDITION)

https://doi.org/10.1007/s10483-023-2993-9

An artificial viscosity augmented physics-informed neural network for incompressible flow*

Yichuan HE[1], Zhicheng WANG[1,†,‡], Hui XIANG[2], Xiaomo JIANG[1], Dawei TANG[1,†,‡]

1. Key Laboratory of Ocean Energy Utilization and Energy Conservation of Ministry of Education, School of Energy and Power Engineering, Dalian University of Technology, Dalian 116024, Liaoning Province, China;
2. Baidu.com Times Technology (Beijing) Co., Ltd., Beijing 100080, China

(Received Nov. 12, 2022 / Revised Mar. 29, 2023)

Abstract Physics-informed neural networks (PINNs) are proved methods that are effective in solving some strongly nonlinear partial differential equations (PDEs), e.g., Navier-Stokes equations, with a small amount of boundary or interior data. However, the feasibility of applying PINNs to the flow at moderate or high Reynolds numbers has rarely been reported. The present paper proposes an artificial viscosity (AV)-based PINN for solving the forward and inverse flow problems. Specifically, the AV used in PINNs is inspired by the entropy viscosity method developed in conventional computational fluid dynamics (CFD) to stabilize the simulation of flow at high Reynolds numbers. The newly developed PINN is used to solve the forward problem of the two-dimensional steady cavity flow at $Re = 1\,000$ and the inverse problem derived from two-dimensional film boiling. The results show that the AV augmented PINN can solve both problems with good accuracy and substantially reduce the inference errors in the forward problem.

Key words physics-informed neural network (PINN), artificial viscosity (AV), cavity driven flow, high Reynolds number

Chinese Library Classification O241
2010 Mathematics Subject Classification 68T01

1 Introduction

The principle of fluid flow and heat transfer problem is widely applied in aerospace, mechanical, and chemical processes. The accurate simulation of the flow and heat transfer process is of great significance in the development of these fields. Computational fluid dynamics (CFD)

∗ Citation: HE, Y. C., WANG, Z. C., XIANG, H., JIANG, X. M., and TANG, D. W. An artificial viscosity augmented physics-informed neural network for incompressible flow. *Applied Mathematics and Mechanics* (*English Edition*), **44**(7), 1101–1110 (2023) https://doi.org/10.1007/s10483-023-2993-9

† Corresponding authors, E-mails: zhicheng_wang@dlut.edu.cn; dwtang@dlut.edu.cn

‡ Zhicheng WANG and Dawei TANG contributed equally to this work

Project supported by the Fundamental Research Funds for the Central Universities of China (No. DUT21RC(3)063), the National Natural Science Foundation of China (No. 51720105007), and the Baidu Foundation (No. ghfund202202014542)

©The Author(s) 2023

employs the finite element method, the finite difference method, or the finite volume method to solve the discrete Naiver-Stokes equation[1], and has traditionally been used to tackle the problems in flow and heat transfer with good accuracy. However, the CFD method usually requires significant computational resources for complex flow processes[2]. Moreover, the data-driven method has achieved transformative impact on science and technology with the development of computing and artificial intelligence technology[3], and has been applied to some difficult physical problems. To this end, if the data-driven method is used as a black box to learn physical information, the results will be difficult to explain or may even violate the laws of physics[4]. Among the data-driven methods, deep neural networks (DNNs) have attracted much attention because of their powerful ability to model complex nonlinear systems. DNNs have been used to solve partial differential equations (PDEs) for better understanding of physics[5]. Specifically, the physics-informed neural networks (PINNs) proposed by Raissi et al.[6], which encode the governing equations of the physical problem in the DNNs, have been used to solve physical problems in various research areas[7].

PINNs solve the governing equations with initial and boundary conditions on the discrete residual points of the domain. They are less restrictive compared with CFD which relies on good-quality meshes and usually requires a significant amount of labor. Using the vorticity-stream function form of the Navier-Stokes equation, Jin et al.[8] developed a PINN to predict the flow field. Based on the experimental temperature data obtained by using tomographic background oriented schlieren (Tomo-BOS), Cai et al.[9] employed a PINN to infer the entire thermal flow field. It has been found that the PINN's ability to predict is greatly affected by training. Many researchers have worked to optimize PINNs to reduce the training time and improve the prediction accuracy. Sun et al.[10] coded the boundary conditions into the PINN in a "hard" way, and proposed the so-called "hard" boundary physical information neural network (HPINN). Their results showed that the HPINN could effectively accelerate the training process and improve the training accuracy to a certain extent. Rao et al.[11] proposed a hybrid variable PINN to simulate the incompressible laminar flow. Taking the flow function as the output of the neural network can automatically satisfy the continuity equation, thus accelerating the training process. McClenny and Braga-Neto[12] proposed the adaptive PINN, which used a soft attention mechanism to accurately fit the stubborn spots in the solution to stiff PDEs. However, all the above PINNs can only improve the accuracy of prediction for specific equations or in certain application scenarios.

The lid-driven cavity flow as a benchmark problem has attracted much attention in PINNs[13]. The Reynolds number Re is the characteristic parameter of the cavity flow, and it is widely accepted that the cavity flow is steady when $Re < 5\,000$[14]. It is the ideal model for validating and studying the accuracy and efficiency of numerical methods as well as PINNs. However, to the best of the authors' knowledge, it has not been reported that state-of-the-art PINNs can solve the cavity flow problem at $Re > 500$[15–17] with good accuracy.

In traditional CFD methods, the artificial viscosity (AV) has been proved to be an efficient numerical "trick" for addressing the numerical instability in solving the Navier-Stokes equation at a high Reynolds number. In this paper, the AV is introduced in the PINNs to improve the accuracy and stability of the prediction. To this end, an AV augmented PINN will be applied to the cavity flow at $Re = 1\,000$.

2 AV augmented PINN

2.1 PINN method

Suppose that a PINN is used to solve the following PDEs:

$$\boldsymbol{u}_t + \mathcal{N}_{\boldsymbol{x}}(\boldsymbol{u}) = 0, \quad \boldsymbol{x} \in \Omega, \quad t \in [0, T], \tag{1}$$

$$\boldsymbol{u}(\boldsymbol{x},0)=h(\boldsymbol{x}),\quad \boldsymbol{x}\in\Omega, \tag{2}$$

$$\boldsymbol{u}(\boldsymbol{x},t)=g(\boldsymbol{x},t),\quad \boldsymbol{x}\in\partial\Omega,\quad t\in[0,T], \tag{3}$$

where $\mathcal{N}_{\boldsymbol{x}}$ represents a linear or nonlinear operation, $\boldsymbol{x}$ and t represent the spatial information and the time information, respectively, Ω and $\partial\Omega$ represent the internal region and the regional boundary of calculation, respectively, $\boldsymbol{u}(\boldsymbol{x},t)$ is the solution to the PDE, $h(\boldsymbol{x})$ is the initial condition, and $g(\boldsymbol{x},t)$ is the boundary condition.

In the PINN, $\boldsymbol{u}(\boldsymbol{x},t)$ is approximated by a fully connected network that takes $(\boldsymbol{x},t)$ as its input and $\boldsymbol{u}_{NN}(\boldsymbol{x},t)$ as the output. The fully connected network consists of multiple hidden layers where the output is $Y^L=[y_1^L,y_2^L,\cdots,y_m^L]$ for each y_j^L,

$$y_j^L=\sigma\Big(\sum_{i=1}^{n}w_{i,j}^L y_i^{L-1}+b_j^L\Big). \tag{4}$$

In the above equation, $w_{i,j}$ and b_j are the weight and the bias of the hidden layer L, respectively, which will be updated after training. σ is the activation function. Note that the commonly used activation functions include sigmoid, ReLu, hyperbolic tangent (Tanh), Softmax, Switch, and Gaussian error linear unit (GELU). The trainable parameters are updated through the back-propagation algorithm, with the goal of minimizing the loss function. As shown in Fig. 1, the PINN combines the physical law and data by means of the following loss function:

$$L=L_{\mathrm{r}}+L_{\mathrm{b}}+L_0, \tag{5}$$

where

$$L_{\mathrm{r}}=\frac{1}{N_{\mathrm{r}}}\sum_{i=1}^{N_{\mathrm{r}}}|\boldsymbol{u}_t(\boldsymbol{x}^i,t^i)+\mathcal{N}_{\boldsymbol{x}}(\boldsymbol{u}(\boldsymbol{x}^i,t^i))|^2, \tag{6}$$

$$L_{\mathrm{b}}=\frac{1}{N_{\mathrm{b}}}\sum_{i=1}^{N_{\mathrm{b}}}|\boldsymbol{u}_t(\boldsymbol{x}^i,t^i)-g^i|^2, \tag{7}$$

$$L_0=\frac{1}{N_0}\sum_{i=1}^{N_0}|\boldsymbol{u}_t(\boldsymbol{x}^i,t^i)-h^i|^2, \tag{8}$$

where L_{r} is the loss of the governing equation on the residual points, L_{b} is the loss on the boundary, and L_0 is the loss of the initial condition. N_{r}, N_{b}, and N_0 are the numbers of the

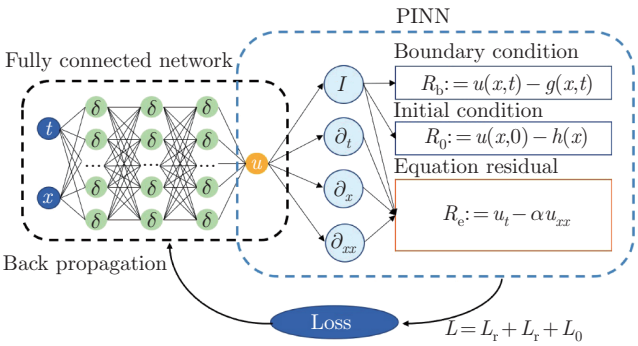

Fig. 1 Schematic diagram of the PINN framework (color online)

residual points of the corresponding loss functions. Moreover, when new data, e.g., experimental measurements in any location of the domain, arrive, an additional loss function can be built to consider the new data information as follows:

$$L_{\text{data}} = \frac{1}{N_{\text{d}}} \sum_{i=1}^{N_{\text{d}}} |\boldsymbol{u}_t(\boldsymbol{x}^i, t^i) - \boldsymbol{u}^i_{\text{data}}|^2. \tag{9}$$

2.2 AV method

In CFD simulation, particularly in the simulation of flow at a high Reynolds number, it is very likely that the mesh resolution will not be able to capture all the small-scale but high-frequency motions, which is a source of numerical error. To this end, the AV method is proposed to smooth out the numerical solution and use the dissipation mechanism of the viscous effect. The incompressible Navier-Stokes equation is

$$\frac{\partial \boldsymbol{u}}{\partial t} + (\boldsymbol{u} \cdot \nabla)\boldsymbol{u} = -\nabla p + \frac{1}{Re}\nabla^2 \boldsymbol{u} \quad \text{in} \quad \Omega. \tag{10}$$

Here, we borrow the idea of the AV to modify the original Navier-Stokes equations, the discrete form of which is smoother on the residual points, and can thus improve the training and eventually create better prediction. Nonetheless, inspired by the work of Wang et al.[18], the residual losses of the two-dimensional Navier-Stokes equations with the AV are given by

$$L_{\text{r1}} = u\frac{\partial u}{\partial x} + v\frac{\partial u}{\partial y} + \frac{\partial p}{\partial x} - \Big(\frac{1}{Re} + \nu_E\Big)\Big(\frac{\partial^2 u}{\partial x^2} + \frac{\partial^2 u}{\partial y^2}\Big), \tag{11}$$

$$L_{\text{r2}} = u\frac{\partial v}{\partial x} + v\frac{\partial v}{\partial y} + \frac{\partial p}{\partial x} - \Big(\frac{1}{Re} + \nu_E\Big)\Big(\frac{\partial^2 v}{\partial x^2} + \frac{\partial^2 v}{\partial y^2}\Big), \tag{12}$$

$$L_{\text{r3}} = \frac{\partial u}{\partial x} + \frac{\partial u}{\partial y}, \tag{13}$$

$$L_{\text{r4}} = \alpha(L_{\text{r1}} \cdot u + L_{\text{r2}} \cdot v) - \nu_E, \tag{14}$$

where u and v represent the velocity components in the x- and y-directions, respectively, p is the pressure, ν_E is the AV, and $\alpha = 0.1$ is a constant.

3 Validation by the benchmark problems

In this paper, the PINN is implemented on the TensorFlow and Baidu PaddleScience libraries, and the PINN training is performed on our local computers, which have a Xeon (R) 6226R CPU@2.90 GHZ, 128 G memory, and Nvidia 3080ti-12G GPU.

3.1 Cavity-driven flow

As a classical CFD problem, the lid-driven cavity flow has been well studied. Although the computational domain and boundary condition are relatively simple, they involve very complex fluid flow characteristics, such as the main vortex, the secondary vortex, the shear flow, and the boundary layer. Therefore, this problem is a frequently used benchmark case to validate the method and code. The studies presented in Refs. [17] and [19] tested a DNN to solve the cavity flow problem up to $Re = 600$. However, as Re increases, the forward problem of cavity flow is still a great challenge for previous PINNs. Here, we turn to the AV augmented PINN, which consists of six hidden layer neural networks, with 80 neurons in each layer. During PINN training, the Adam optimizer, 40 000 residual points for the governing equations, and 4×256 residual points for the boundary conditions, are employed. In the total of $100\,000 + 100\,000 + 100\,000 + 150\,000 + 150\,000$ epochs, the learning rates 1×10^{-3}, 5×10^{-4},

1×10^{-4}, 1×10^{-5}, and 1×10^{-6} are used, respectively. It is worth noting that, with the same hyper-parameters, the PINN simulation is performed five times. The time history of loss from Simulation 1 is plotted in Fig. 2, where loss-bcs. is the loss of the boundary condition, and loss-equ. is the loss of the Navier-Stokes equations. The results shown in Figs. 3–5 are from Simulation 1.

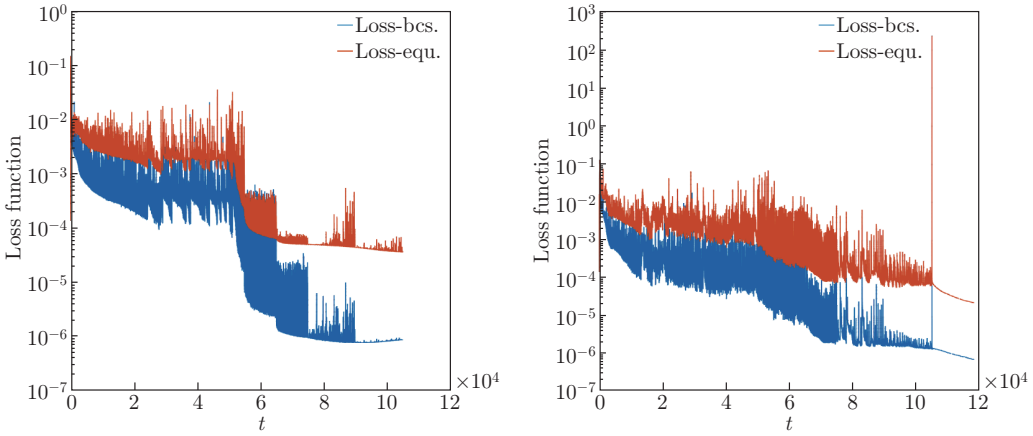

Fig. 2 Time series of the training loss of the PINN at $Re = 1\,000$ (color online)

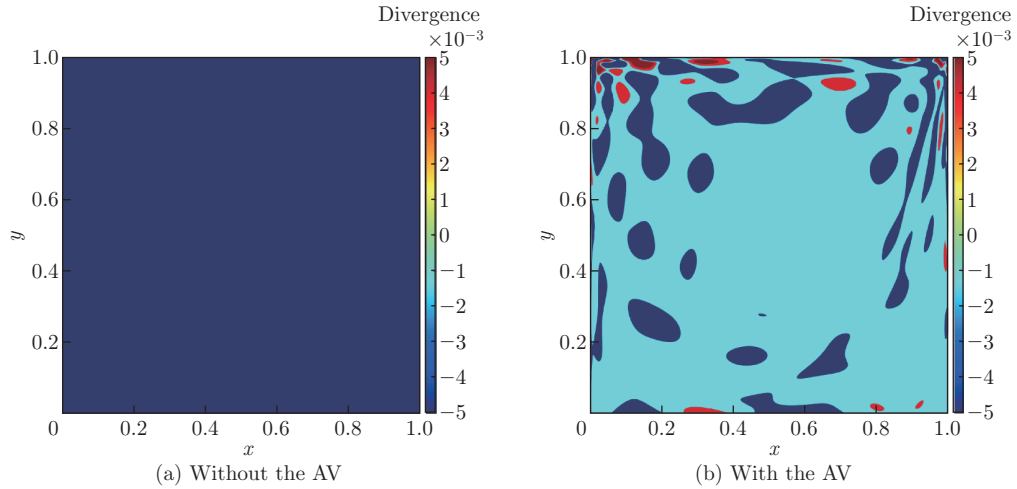

Fig. 3 Comparison of the PINN prediction and reference data on divergence (color online)

Table 1 shows the root mean square error between the PINN prediction and the reference value that is obtained by the high-fidelity simulation using the high-order spectral element method. It can be observed that using the original Navier-Stokes equation, the PINN prediction error is more than 80%, and is reduced to less than 20% when the AV is employed. In particular, in Simulation 3, the error is less than 6%. It can be seen that the equation loss of the PINN can be reduced to the order of 10^{-5}, while the final loss of the boundary condition is on the order of 10^{-6}. In addition, the final value of the loss function between the PINN with and without the AV is comparable, although the predicted error has notable difference. In the simulation of an

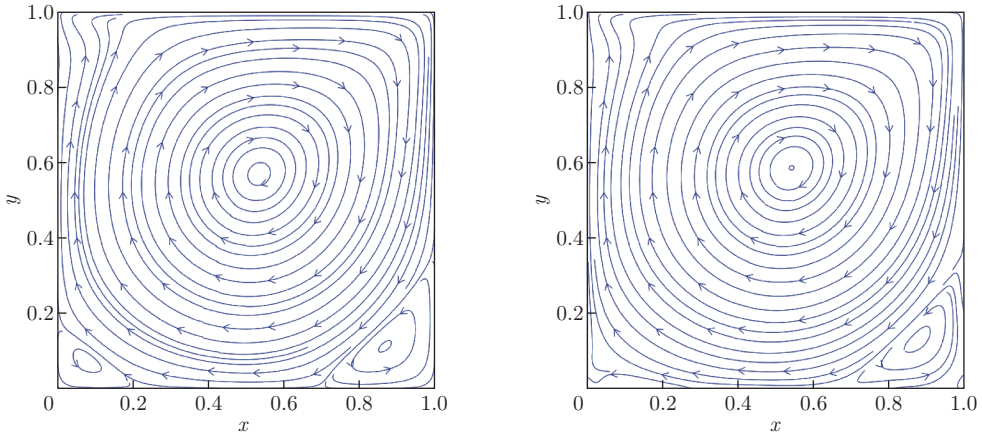

(a) Reference data on the streamlines

(b) PINN prediction on the streamlines where the AV is used

Fig. 4 Comparison of the PINN prediction and reference data on the streamlines (color online)

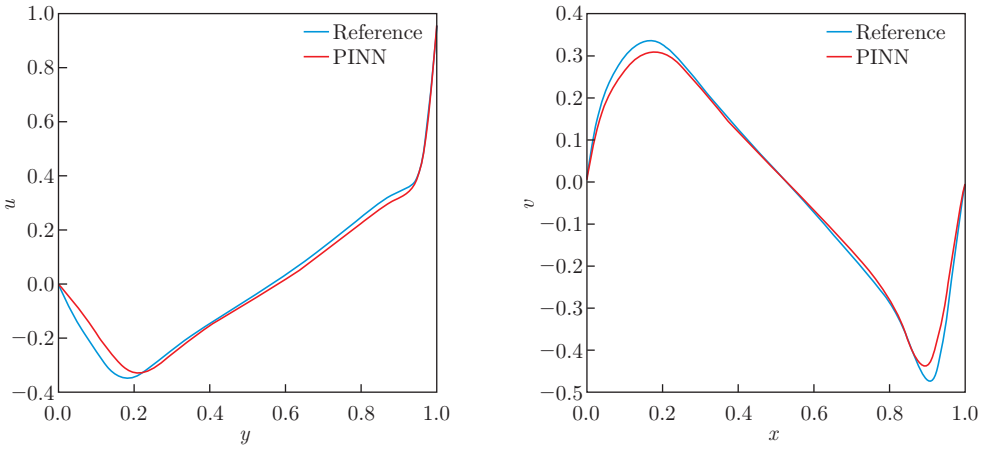

(a) u profile at $x=0.5$

(b) v profile at $y=0.5$

Fig. 5 Comparison of the PINN prediction and reference data on the velocity profiles (color online)

incompressible flow, the prediction accuracy can be represented by the velocity divergence, and a large absolute value of the divergence indicates that the method has poor prediction accuracy. Figure 3 shows the comparison of the PINN prediction on the divergence with and without the AV. It could be found that the AV can substantially reduce the velocity divergence.

In the cavity flow with an increasing Re, a second-order vortex will be formed in the left and right lower corners of the square cavity, owing to the viscous effect of the solid wall. In Fig. 4, compared with the reference data, the PINN prediction shows the vortex on the right bottom well, while it barely predicts the smaller one on the left bottom. As the figure shows, the vortex cannot be predicted in the left corner. Because there is so little known information that can be used to speculate on the vortex in the left corner, creating the PINN does not solve the vortex prediction problem. Figures 5(a) and 5(b) plot the comparison of the PINN prediction and the reference data on the velocity profiles at $x = 0.5$ and $y = 0.5$, respectively. It can be observed that the PINN with the AV can predict the velocity with acceptable accuracy.

Table 1 Mean square error (%) between the PINN prediction and the reference value for the two-dimensional cavity flow at $Re = 1\,000$

Simulation	With the AV			Without the AV		
	u	v	p	u	v	p
1	10.28	9.72	10.72	85.86	83.17	87.99
2	16.52	14.31	13.25	85.08	82.51	86.14
3	19.49	19.18	23.37	83.74	81.39	83.63
4	3.12	3.34	5.72	83.89	81.50	84.04
5	16.12	16.66	22.37	82.10	80.06	80.82

3.2 Film boiling

We now focus on the two-dimensional film boiling problem. The objective of this section is to demonstrate the feasibility of using the PINN to predict an unsteady complex flow in a deformed domain. The film boiling problem was documented in Ref. [20] as follows: initially, a thin vapor film covered the bottom wall and under the liquid. The wall temperature was kept at T_{w}, which was higher than the liquid saturation temperature and resulted in a phase change at the vapor-liquid interface, causing heat to be absorbed from the wall through the vapor to the liquid. Therefore, the interface was pushed upward. The higher density of the liquid above the vapor triggered the Rayleigh-Taylor instability, magnified the interface disturbance, and eventually led to rising bubbles. Note that film boiling is a complex two-phase flow, but the PINN assumed that the interface was known such that the two-phase flow could be simplified as two single-phase flows, one of which was in the vapor, and the other was in the liquid. In this paper, we consider the flow in the vapor only. Nonetheless, in this section, the data for the PINN are obtained from the high-fidelity simulation by using the improved phase field method[20]. The thermophysical properties of the vapor in the simulation are shown in Table 2. Note that the vapor-liquid interface is a known boundary from the PINN's perspective, and to predict the unsteady flow, 350 snapshots of the vapor-liquid interface are used. In addition, it is assumed that the PINN can access the velocity data at five random points within the vapor. The structure of the neural networks is the same as that in the previous section, but during training, $200+200+200+200+200$ epochs with the learning rates 1×10^{-3}, 2×10^{-4}, 1×10^{-4}, 5×10^{-5}, and 1×10^{-5} are used.

Table 2 Thermophysical properties by two-dimensional film boiling

Parameter	Value	Definition
ρ_{v}	5 kg/m^3	Gas density
ρ_{l}	200 kg/m^3	Liquid density
μ_{v}	5 mPa·s	Gas viscosity
μ_{l}	100 mPa·s	Liquid viscosity
C_{pv}	200 J/(kg·K)	Gas heat capacity
C_{pl}	400 J/(kg·K)	Liquid heat capacity
k_{v}	1 W/(m·K)	Gas thermal conductivity
k_{l}	40 W/(m·K)	Liquid thermal conductivity
T_{sat}	500 K	Saturation temperature
h_{lv}	104 J/kg	Latent heat

In summary, the errors between the PINN prediction and the reference data on the velocities u and v and the pressure p are 3.5%, 5.8%, and 9.6%, respectively. Figure 6 compares the PINN prediction of u, v, and p at $t = 1.0$ and the corresponding reference data. It can be observed that for the velocity, the error is mainly concentrated in the thin film close to the wall and in the bottleneck of the bubble, where drastic changes in the velocity and the pressure exist.

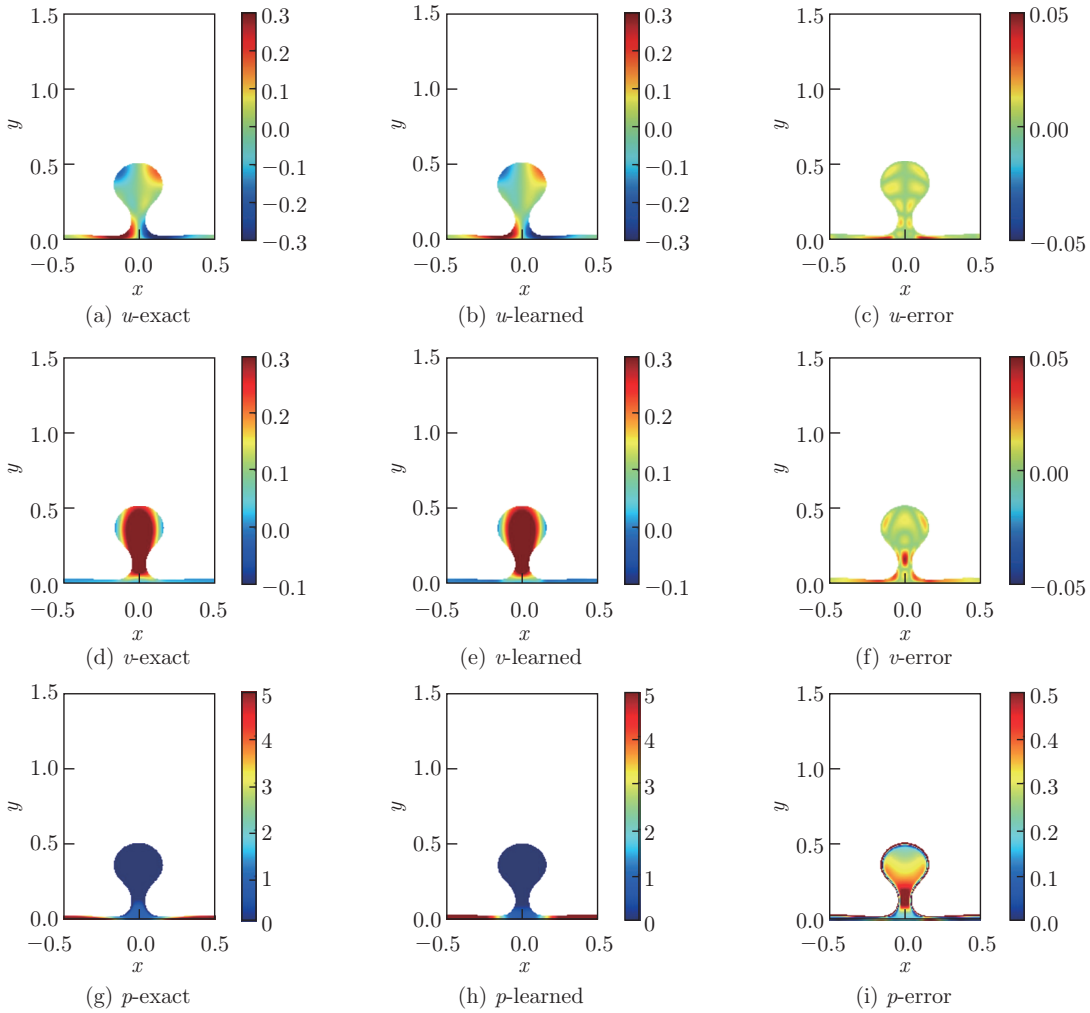

Fig. 6 Prediction of film boiling results by the PINN with the AV (color online)

4 Conclusions

In this paper, an AV augmented PINN is proposed to improve the flow prediction at moderate or high Reynolds numbers. The newly developed PINN is validated by solving the forward problem of a steady two-dimensional lid-driven cavity flow at $Re = 1\,000$ and the unsteady inverse problem of film boiling. The results show that the AV can substantially improve the accuracy of the PINN prediction in both forward and inverse problems.

Conflict of interest The authors declare no conflict of interest.

Open access This article is licensed under a Creative Commons Attribution 4.0 International License, which permits use, sharing, adaptation, distribution and reproduction in any medium or format, as long as you give appropriate credit to the original author(s) and the source, provide a link to the Creative Commons licence, and indicate if changes were made. To view a copy of this licence, visit http://creativecommons.org/licenses/by/4.0/.

References

[1] QIANG, L. I., YU, G. U., and WANG, H. The influence of temperature on flow-induced forces on quartzcrystal-microbalance sensors in a Chinese liquor identification electronic-nose: three-dimensional computational fluid dynamics simulation and analysis. *Applied Mathematics and Mechanics* (*English Edition*), **40**(9), 1301–1312 (2019) https://doi.org/10.1007/s10483-019-2512-9

[2] LÓPEZ, A., NICHOLLS, W., STICHLAND, M. T., and DEMPSTER, W. M. CFD study of jet impingement test erosion using Ansys Fluent and OpenFOAM. *Computer Physics Communications*, **197**, 88–95 (2015)

[3] JORDAN, M. I. and MITCHELL, T. M. Machine learning: trends, perspectives, and prospects. *Science*, **349**(6245), 255–260 (2015)

[4] KARNIADAKIS, G. E., KEVEREKIDIS, I. G., LU, L., PERDIKARIS, P., WANG, S. F., and YANG, L. Physics-informed machine learning. *Nature Reviews Physics*, **3**(6), 422–440 (2021)

[5] LECUN, Y., BENGIO, Y., and HINTON, G. Deep learning. *nature*, **521**(7553), 436–444 (2015)

[6] RAISSI, M., PERDIKARIS, P., and KARNIADAKIS, G. E. Physics-informed neural networks: a deep learning framework for solving forward and inverse problems involving nonlinear partial differential equations. *Journal of Computational Physics*, **378**, 686–707 (2019)

[7] RAISSI, M., YAZDANI, A., and KARNIADAKIS, G. E. Hidden fluid mechanics: learning velocity and pressure fields from flow visualizations. *Science*, **367**(6481), 1026–1030 (2020)

[8] JIN, X. W., CAI, S. C., LI, H., and KARNIADAKIS, G. E. NSFnets (Navier-Stokes flow nets): physics-informed neural networks for the incompressible Navier-Stokes equations. *Journal of Computational Physics*, **426**, 109951 (2021)

[9] CAI, S. Z., WANG, Z. C., FUEST, F., JIN, J. Y., CALLUM, G., and KARNIADAKIS, G. E. Flow over an espresso cup: inferring 3-D velocity and pressure fields from tomographic background oriented schlieren via physics-informed neural networks. *Journal of Computational Physics*, **915**, A102 (2021)

[10] SUN, L. N., GAO, H., PAN, S. W., and WANG, J. X. Surrogate modeling for fluid flows based on physics-constrained deep learning without simulation data. *Computer Methods in Applied Mechanics and Engineering*, **361**, 112732 (2020)

[11] RAO, C. P., SUN, H., and LIU, Y. Physics-informed deep learning for incompressible laminar flows. *Theoretical and Applied Mechanics Letters*, **10**(3), 207–212 (2020)

[12] MCCLENNY, L. and BRAGA-NETO, U. Self-adaptive physics-informed neural networks using a soft attention mechanism. *arXiv Preprint*, arXiv: 2009.04544 (2020) https://doi.org/10.48550/arXiv.2009.04544

[13] BOTELLA, O. and PEYRET, R. Benchmark spectral results on the lid-driven cavity flow. *Computers and Fluids*, **27**(4), 421–433 (1998)

[14] BISWAS, S. and KALITA, J. C. Topology of corner vortices in the lid-driven cavity flow: 2D vis a vis 3D. *Archive of Applied Mechanics*, **90**(3), 2201–2216 (2020)

[15] JAGTAP, A. D., KHARAZMI, E., and KARNIADAKIS, G. E. Conservative physics-informed neural networks on discrete domains for conservation laws: applications to forward and inverse problems. *Computer Methods in Applied Mechanics and Engineering*, **365**, 113028 (2020)

[16] BAI, X., WANG, Y., and ZHANG, W. Applying physics informed neural network for flow data assimilation. *Journal of Hydrodynamics*, **32**(6), 1050–1058 (2020)

[17] CHIU, P. H., WONG, J. C., OOI, C., DAO, M. H., and ONG, Y. S. CAN-PINN: a fast physics-informed neural network based on coupled automatic numerical differentiation method. *Computer Methods in Applied Mechanics and Engineering*, **395**, 114909 (2022)

[18] WANG, Z., TRIANTAFYLLOU, M. S., CONSTANTINIDES, Y., and KARNIADAKIS, G. E. An entropy-viscosity large eddy simulation study of turbulent flow in a flexible pipe. *Journal of Fluid Mechanics*, **859**, 691–730 (2019)

[19] CHEN, X. H., CHEN, R. L., WAN, Q., XU, R., and LIU, J. An improved data-free surrogate model for solving partial differential equations using deep neural networks. *Scientific Reports*, **11**, 19507 (2021)

[20] WANG, Z., ZHENG, X., CHRYSSOSTOMIDIS, C., and KARNIADAKIS, G. E. A phase-field method for boiling heat transfer. *Journal of Computational Physics*, **435**, 110239 (2021)